Original Article

Effect of electrohydrodynamic printing scaffold with different spacing on chondrocyte dedifferentiation

Xincheng Liu[1#^], Zhao Zhang[1#], Yubo Shi[1], Xingxing Meng[2], Zhennan Qiu[3,4], Xiaoli Qu[3,4], Jingyi Dang[1], Yushen Zhang[1], Liguo Sun[1,5], Lei Wang[1], Dongze Zhu[1], Zhenzhou Mi[1], Jiankang He[3,4], Hongbin Fan[1]

[1]Department of Orthopedic Surgery, Xijing Hospital, the Fourth Military Medical University, Xi'an, China; [2]Department of Aerospace Hygiene, the Fourth Military Medical University, Xi'an, China; [3]State Key Laboratory for Manufacturing Systems Engineering, Xi'an Jiaotong University, Xi'an, China; [4]Rapid Manufacturing Research Center of Shaanxi Province, Xi'an Jiaotong University, Xi'an, China; [5]Shaanxi Province Hospital of Traditional Chinese Medicine, Xi'an, China

Contributions: (I) Conception and design: X Liu, Z Zhang, H Fan; (II) Administrative support: X Qu, J He, H Fan; (III) Provision of study materials or patients: Z Qiu; (IV) Collection and assembly of data: X Liu, X Meng, X Qu; (V) Data analysis and interpretation: X Liu, Z Zhang; (VI) Manuscript writing: All authors; (VII) Final approval of manuscript: All authors.

[#]These authors contributed equally to this work and should be considered as co-first authors.

Correspondence to: Hongbin Fan. Department of Orthopedic Surgery, Xijing Hospital, the Fourth Military Medical University, Xi'an 710032, China. Email: fanhongbin75@yahoo.com.

Background: Osteoarthritis (OA) is a common degenerative disease. Chondrocyte dedifferentiation can accelerate the progress of OA. Three-dimensional printing (3DP) is widely used in tissue regeneration applications. A three-dimensional (3D) culture system with 3D printed scaffolds could reduce the dedifferentiation of chondrocytes during passages, which would be a potential method for chondrocyte expansion.

Methods: The viability and proliferation of chondrocytes on scaffolds and effects of scaffolds with 100, 150, 200, 250 or 300 μm spacing on chondrocyte dedifferentiation were analyzed *in vitro*. The morphology of scaffolds and cell/scaffold constructs was observed by scanning electron microscopy (SEM). Glycosaminoglycan (GAG) was evaluated by Alcian blue staining. The effects of different spacing on chondrocyte dedifferentiation were evaluated by the messenger RNA (mRNA) and protein levels of cartilage-related genes.

Results: With more binding sites, the proliferation and viability of chondrocytes on scaffolds with 100 and 150 μm spacing were better than those with 200, 250 and 300 μm spacing on day 1, but this advantage diminished over time. The histology and quantitative real-time polymerase chain reaction (qRT-PCR) results showed that 200 μm spacing inhibits chondrocyte dedifferentiation better.

Conclusions: 3D printed scaffolds with 200 μm spacing can inhibit chondrocyte dedifferentiation, providing a basis for the future study of 3D printed scaffolds as an effective method for chondrocyte expansion.

Keywords: Osteoarthritis (OA); electrohydrodynamic printing (EHDP); tissue engineering (TE); chondrocyte dedifferentiation; chondrocytes

Submitted May 07, 2022. Accepted for publication Jul 06, 2022.
doi: 10.21037/atm-22-2796
View this article at: https://dx.doi.org/10.21037/atm-22-2796

^ ORCID: 0000-0001-5065-7017.

Introduction

Articular cartilage lacks self-healing ability if injured (1,2), which may initiate the progression of osteoarthritis (OA). OA is a clinical syndrome that most commonly affects the knee and hip joints; it is a painful condition that leads to a reduction in physical function and quality of life (3,4). Non-steroidal anti-inflammatory drugs, acetaminophen, and opioids are most commonly used to treat the pain associated with OA, with limited effectiveness (5). At present, there is no approved disease-releasing drug available to treat OA (6), and current management strategies that are typically limited to the late stages of OA lead to joint replacement (7,8). Tissue engineering (TE) is a promising option for the surgical replacement of defective tissues (9).

Autologous chondrocyte implantation, which requires numerous articular chondrocytes (ACs), is a prospective treatment method for OA. ACs are extracted from cartilage in articular joints and could be expanded *in vitro* to obtain a sufficient number of cells (10). It has been demonstrated that chondrocytes cultured in flasks lose their typical phenotype and subsequently undergo dedifferentiation (11). Their morphology usually changes from polygon into fibroblast-like cells that produce type-I collagen instead of type-II collagen during the proliferation of repeated passaging, which influences their function in cartilage TE (CTE) (12,13). Hypoxia, specific cytokines (14), and mechanical loadings (15) are applied to inhibit chondrocyte dedifferentiation but have limited application because of the complex methods and experimental conditions involved.

Three-dimensional printing (3DP) has shown enormous potential in tissue regeneration applications, which could be attributed to the ease of fabrication of patient-customized scaffolds (16). With the expansion of 3DP technologies into TE, new tools have been provided to researchers to independently control and optimize the properties of scaffolds (17). 3DP technology could create complex structures on medical image-based and computer-aided design, which could be potentially used in the musculoskeletal system, especially owing to their flexibility, reproducibility, and ease of use (18,19). Three-dimensional (3D) culture on 3DP scaffolds can effectively induce dedifferentiated chondrocytes to become functional, redifferentiated chondrocytes, enabling them to regenerate mature cartilage (20). It has been demonstrated that high-cell-density 3D cultures support the redifferentiation of dedifferentiated ACs (21). Electrohydrodynamic printing (EHDP) is a technique that uses electric fields rather than thermal or acoustic energy, which can create fluid flow for delivering inks to a substrate (22,23). It is compatible with a variety of materials, and the high printing speeds maintain a low system cost (23,24). The capability and specification of 3D printers are continually evolving from the initial printer using one type of material, whereas multiple material extrusion is now possible (25). With these benefits, electrohydrodynamic-printed scaffolds would be a potential CTE method. With the different structures of porosity, spacing, roughness, or surface micro- and nano-topography, the scaffolds would exhibit different biomechanical, cell adhesion, cell distribution, cell infiltration, cell proliferation, and differentiation properties (26-30). However, the specific indicator of 3D printed scaffolds for CTE remains unclear. Spacing is one of the most important parameters in 3DP, which determines the life space of cells and the secretion of extracellular matrix (ECM); it has been discussed in numerous studies (31-35), but the conclusions are not consistent. Small pore size scaffolds (100–200 μm) are more conducive to chondrogenesis (32); however, Prasopthum *et al.* (33) recommended a scaffold size of 200–700 μm for chondrogenesis during osteochondral regeneration. Meanwhile, a spacing size <200 μm has not been adequately investigated. Moreover, chondrocytes cultured on scaffolds with different spacing sizes have not been discussed previously, and research into chondrocyte dedifferentiation is inadequate.

In this study, the effect of EHDP grid-like scaffolds with different spacing (100, 150, 200, 250, or 300 μm) on chondrocyte dedifferentiation *in vitro* was investigated, which offers a potential method for chondrocyte expansion and provides benefits for the design of scaffolds. Specifically, the properties of materials, the viability and proliferation of cells, and the process of chondrocyte dedifferentiation were investigated. We present the following article in accordance with the MDAR reporting checklist (available at https://atm.amegroups.com/article/view/10.21037/atm-22-2796/rc).

Methods

Materials

Medical-grade polycaprolactone (PCL) [molecular weight (MW) =80,000 g/moL] was purchased from Jinan Daigang Biomaterial (Jinan, China). Trypsin digestion solutions [0.25% ethylenediaminetetraacetic acid (EDTA) with phenol red; #PC-90001], penicillin-streptomycin solution

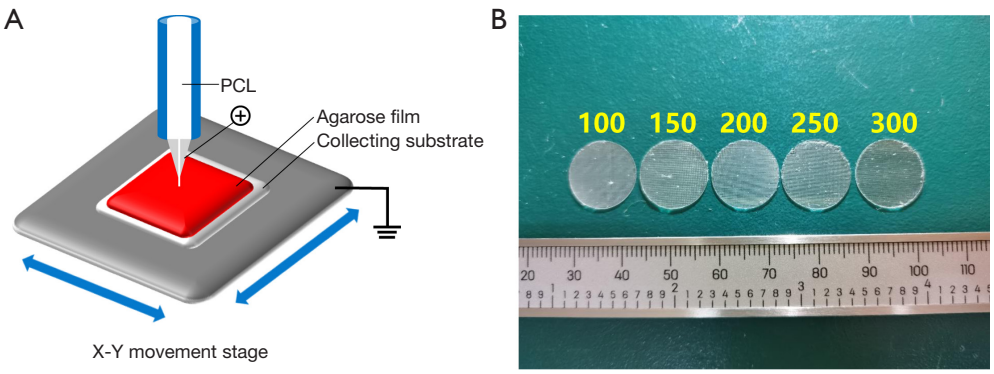

Figure 1 Schematic of the electrohydrodynamic 3DP to fabricate PCL scaffolds (A) and general pictures of the scaffolds with different spacing (unit: μm) (B). PCL, polycaprolactone; 3DP, three-dimensional printing.

(100X; #PC-86115), and collagenase type II (#PC-50995) were purchased from PlantChemMed Biology Co., Ltd. (Shanghai, China). 4',6-diamidino-2-phenylindole (DAPI) were purchased from Solarbio (Beijing, China). Growth medium and fetal bovine serum (FBS) were purchased from Gibco (Grand Island, NY, USA) for cell culture. Alamar blue was purchased from Gibco for cellular activities testing. IFluor^{TM} 488 phalloidin was purchased from Yeason (Shanghai, China) for cytoskeleton staining. The live/dead viability/cytotoxicity kit was purchased from Invitrogen (Carlsbad, CA, USA). Anti-aggrecan antibody (#ab36861), anti-collagen II antibody (#ab34712), and anti-SOX9 antibody (#ab185966) were purchased from Abcam (Abcam, Cambridge, MA, USA) for immunofluorescence. CoraLite488-conjugated Affinipure Goat Anti-Rabbit immunoglobulin G (IgG) (H + L) was purchased from Proteintech (Wuhan, China) for immunofluorescence. Total RNA kit I (#R6834) was purchased from Omega Bio-Tek (Norcross, GA, USA) for total RNA extraction. PrimeScript RT Master Mix (#RR036A) and TB Green Premix Ex Taq II (Tli RNaseH Plus; #RR820A) were purchased from TaKaRa (Kusatsu, Shiga, Japan) for quantitative real-time polymerase chain reaction (qRT-PCR). All other reagents were analytical grade.

Fabrication of microscale PCL scaffolds

The diagrammatic figure for the fabrication of PCL scaffolds is shown in *Figure 1*, as reported in our previous study (36). Briefly, PCL chippings were loaded into a glass and stainless-steel syringe immersed in a water circulating system with a controlled temperature, which was increased to 90 ℃ to melt the PCL. The printing nozzle (diameter of 350 μm) was grounded to initialize the EHDP process. A glass collector mounted onto an XY moving stage was connected with the positive terminal of a high voltage generator. The electric field force between the collector and the nozzle induces the EHDP of tiny filaments, and a specific pattern is obtained by controlling the movement of the XY stage. On this basis, a 3D fibrous scaffold would be jetted with the stacking of tiny filaments in a layer-by-layer manner.

In this study, the nozzle-to-collector distance, moving speed, voltage, and air pressure were fixed at 3 mm, 25 mm/s, 3.15 kV, and 300 Pa, respectively. The spacing of scaffolds was set as 100 μm (group 100), 150 μm (group 150), 200 μm (group 200), 250 μm (group 250), and 300 μm (group 300). For further *in vitro* experiments, a thin layer of agarose film was coated on the glass slide, which could inhibit cell adherence on the glass surface. Meanwhile, a PCL membrane was made by adequate volatilization in a 24-well plate of a solution containing 10% w/v of PCL in acetic acid as the control (Con) group.

Isolation and expansion of chondrocytes

Cartilage tissues were obtained from the femoral heads and knee joints in 3-week-old female SD rats purchased from the Experimental Animal Center of the Fourth Military Medical University (Xi'an, China). They were washed in phosphate-buffered saline (PBS) and chopped. Chondrocytes were then isolated by 5-minute enzymatic digestion with 0.05% trypsin and enzymatic digestion with 0.2% type II collagenase overnight. The cells were expanded in a growth medium containing 2.5 μg/mL Amphotericin B and 0.1 mg/mL streptomycin with

10% FBS. Upon reaching 70–80% confluence, adherent cells were freed from the flask with 0.05% trypsin and subcultured. All assays were performed on chondrocytes of passage 2. All animal experiments were approved by the Fourth Military Medical University Animal Ethics Committee (permission number: IACUC-20220701) and were implemented in accordance with the Guide for the Care and Use of Laboratory Animals (NIH, 8th edition).

Cell culture on PCL scaffolds

PCL membranes and microscale PCL scaffolds with different spacing were sterilized in a 75% alcohol solution for 60 min, followed by ultraviolet irradiation overnight. Next, the scaffolds were washed with PBS three times and moved into a 24-well plate. The chondrocytes were seeded on the scaffold at a density of 3×10^4 cells in each pore. After chondrocyte attachment for 30 min, 1 mL of fresh culture medium was added to each well. The culture medium was replaced every 3 days.

Morphology of scaffolds

Scanning electron microscopy (SEM; S3400, Hitachi, Japan) was applied to observe the scaffold and cell/scaffold. After culturing for 7 days, the cell/scaffold constructs were collected, washed three times with PBS, fixed in 2.5% (v/v) glutaraldehyde for 1 day, followed by dehydration with graded ethanol. Next, the scaffolds and cell/scaffold constructs were coated with gold with a Sputter Coater for 1 min at a current of 30 mA and observed with a SEM at a voltage of 5 kV. The spacing of scaffolds in the five groups was measured simultaneously.

Analysis of scaffold biocompatibility, cell viability, and proliferation

The cell/scaffold constructs, which were cultured for 24 h, were stained with live/dead staining for the visualization of cellular morphology and distribution on scaffolds. The staining was visualized and photographed by fluorescence microscopy (Carl Zeiss, Germany). Cell proliferation and viability on the scaffolds were evaluated on days 1, 3, 5, and 7 by Alamar blue colorimetric assay according to the manufacturer's protocol. Briefly, the scaffolds were incubated in 1 mL of growth medium and 0.1 mL Alamar blue solution for 4 h. The fluorescence intensity of the culture media at 560/590 nm was measured in triplicate using a Synergy H1 microplate reader (BioTek, USA).

Alcian blue staining

Glycosaminoglycan (GAG) was evaluated by Alcian blue staining. The cell/scaffold constructs were harvested on day 7. The samples were washed with PBS three times, fixed with 4% (v/v) paraformaldehyde in PBS for 0.5 h, dehydrated through a graded ethanol series, and stained with 1% (w/v) Alcian blue solution in 3% (w/v) glacial acetic acid, pH 4.2, for 0.5 h, followed by washing with tap water for 10 minutes. Finally, the samples were photographed by optical microscopy (Carl Zeiss, Germany).

Actin filament staining

The cell/scaffold constructs in groups were harvested on day 7 for analysis. The samples were washed with PBS three times and then fixed with 4% (w/v) paraformaldehyde in PBS for 0.5 h. The samples were permeabilized with 0.1% Triton X-100 for 10 min and rinsed with PBS three times, stained with iFluor™ 488 phalloidin according to the manufacturer's protocol, and then washed with PBS three times. The samples were incubated with DAPI nuclear stain for 3 min and then washed with PBS three times. Finally, the cellular actin filaments were photographed using a confocal laser scanning microscope (A1, Nikon, Japan).

qRT-PCR

The messenger RNA (mRNA) levels of *AGG*, *Col2a1*, and *SOX9* in the chondrocytes on scaffolds were respectively measured by qRT-PCR analysis. Briefly, total RNA was extracted using a total RNA kit. In total, 1,500 ng of RNA was reverse transcribed by PrimeScript RT Master Mix using the ProFlex PCR system (Life, USA). Subsequently, qRT-PCR was conducted by using TB Green Premix Ex Taq II (Tli RNaseH Plus) with a Bio-Rad CFX96 Real-Time PCR system (Bio-Rad, USA). The mRNA expression level was normalized against that of glyceraldehyde-3-phosphate dehydrogenase (*GAPDH*). The primer sequences of target genes were obtained from previous studies (*Table 1*).

Immunofluorescence

The PBS-washed and fixed cell-scaffold constructs were incubated with normal goat serum (1:100) for 10 min at room temperature and then rabbit monoclonal antibody

Table 1 Primer sequences for the qRT-PCR analysis

Gene primer sequences	Forward	Reverse
GAPDH	CCGCATCTTCTTGTGCAGTG	ACCAGCTTCCCATTCTCAGC
AGG	TGAGAGAGGCGAATGGAACG	TTCTGCCCGAGGGTTCTAGC
Col2a1	GCCAGGATGCCCGAAAATTAG	CTCGTCAAATCCTCCAGCCA
SOX9	CACAAGAAAGACCACCCCGA	TGCACGTCTGTTTTGGGAGT

qRT-PCR, quantitative real-time polymerase chain reaction; *GAPDH*, glyceraldehyde-3-phosphate dehydrogenase; *AGG*, aggrecan.

against AGG (1:200), Col2a1 (1:200), or SOX9 (1:200) at 4 ℃ overnight. Next, the samples were rewarmed at room temperature for 10 min and rinsed with PBS. Subsequently, CoraLite488-conjugated goat anti-rabbit IgG (1:200) was added to the samples for incubation at 37 ℃ for 50 min. Thereafter, the samples were washed with PBS three times, incubated with DAPI nuclear stain for 3 min, and then washed with PBS three times. Immunoreactivity was visualized and photographed using a confocal laser scanning microscope.

Statistical analysis

Graphs were drawn using GraphPad Prism 9 (GraphPad Software, USA) and statistical analyses were performed using SPSS 26 (IBM, USA). Multiple group comparisons were performed using one-way analysis of variance (ANOVA). $P<0.05$ was considered statistically significant.

Results

Morphologies of PCL scaffolds with different spacing

SEM micrographs of the surfaces of PCL scaffolds with different spacing are shown in *Figure 2*. The surfaces of all samples were basically ordered. Groups 200, 250, and 300 were neater than groups 100 and 150. The average spacing of the five groups was 99.28±7.50, 151.21±9.54, 203.60±7.25, 246.17±6.42, and 293.77±7.58 μm, respectively (n=4). The fitness of the printer and the static between the fibers significantly affected the neatness of the scaffolds.

Viability of chondrocytes on scaffolds with different spacing

Figure 3 shows the fluorescence images of chondrocytes based on the live/dead assay for the assessment of the viability of chondrocytes on scaffolds with different spacing for 24 h. Live cells take up fluorescein diacetate, converting the non-fluorescent one into a green fluorescent one. In contrast, propidium iodide cannot pass through a viable cell membrane, which shows red fluorescence for distinguishing living from dead cells (37). Our results found that live cells were observed on each sample, while a small number of dead cells were only visible at the corners of the scaffold, probably due to the lack of contacting growth medium and air.

Cell proliferation on scaffolds with different spacing

On day 1, the proliferation rate of cells cultured in groups 100 and 150 was better than that in groups 200, 250, and 300 ($P<0.001$). Moreover, group 200 was superior to groups 250 and 300 ($P<0.05$). There was no significant difference between groups 100 and 150 or groups 250 and 300. This phenomenon could be caused by smaller spacing offering more cell growth space. The same situation occurred on day 3, but there were no significant differences between groups 200, 250, and 300. On day 5, the proliferation rate of cells in group 200 became higher. There was no difference between groups 100, 150, and 200. On day 7, only the viability of cells cultured in group 100 was better than that in groups 200, 250, and 300 ($P<0.05$). There was no difference between groups 150, 200, 250, and 300 (*Figure 4*). With more binding sites, the proliferation and viability of chondrocytes in groups 100 and 150 were better than that in groups 200, 250, and 300 on day 1, but this superiority diminished over time.

Morphologies of chondrocytes on PCL scaffolds with different spacing

As shown in *Figure 5*, the dark staining of Alcian blue in groups 200, 250, and 300 indicated that more GAG was produced compared to groups 100 and 150. *Figures 2,6* showed that chondrocytes were aggregated at the corner of the scaffolds and gradually extended on the microfibers. In

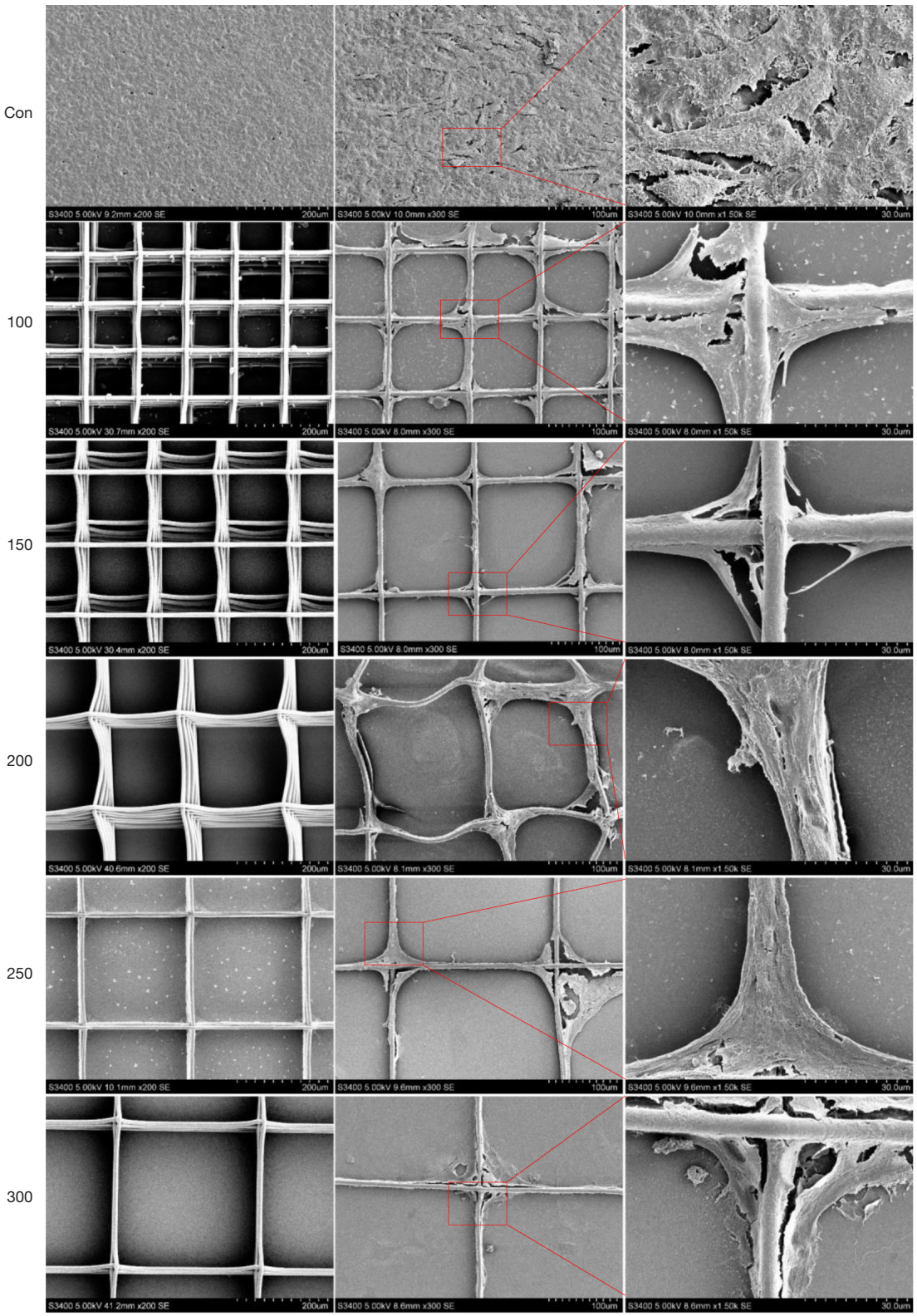

Figure 2 Scanning electron microscope images of the scaffolds and cell/scaffold structures with different spacing. Con, control.

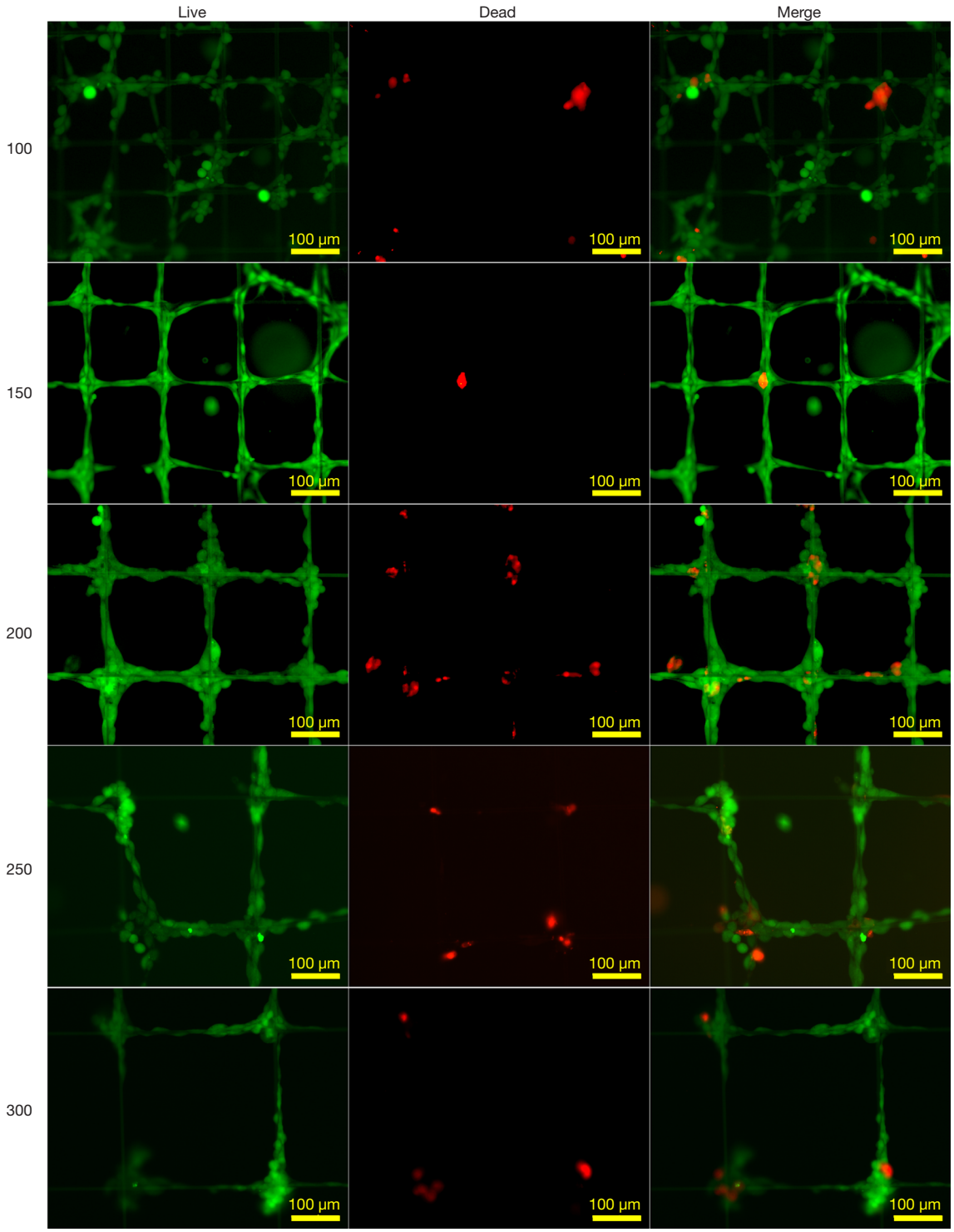

Figure 3 Live/dead imaging of chondrocytes cultured on microfibrous structures with different spacing for 1 day, with a scale bar of 100 μm.

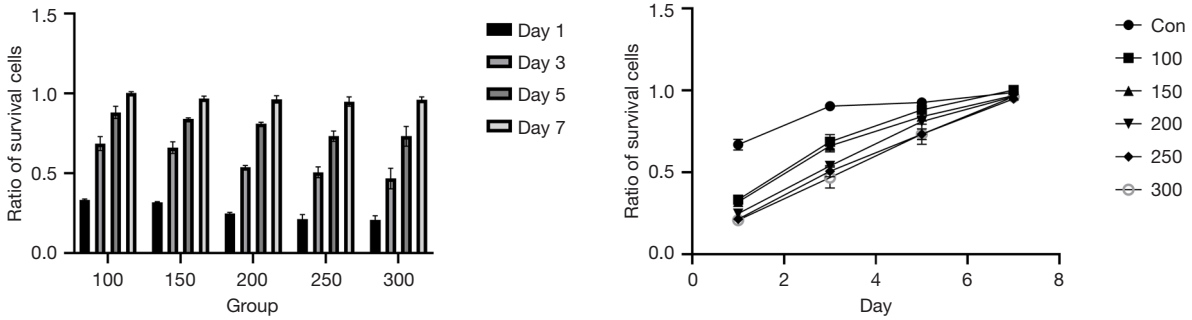

Figure 4 Cellular activities of chondrocytes cultured on microfibrous structures with different spacing were observed using the Alamar blue assay. Con, control.

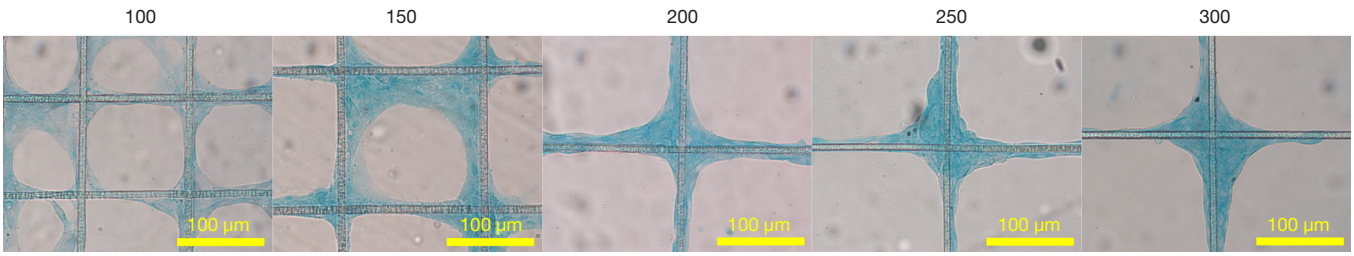

Figure 5 Images of chondrocytes cultured on microfibrous structures with different spacing stained with Alcian blue, with a scale bar of 100 μm.

groups 100 and 150, the cells could fill in the square caves.

Expression of related signalling molecules and proteins

The result of *Figure* 7 indicated that chondrocytes cultured on scaffolds represent better maintenance of the chondrocyte phenotype on both the mRNA and protein levels. Among them, chondrocytes cultured in group 200 exhibited the highest AGG protein levels and mRNA expression of *AGG*, *Col2a1*, and *SOX9* (P<0.001). However, although group 200 still represented more protein of Col2a1 and *SOX9* than group 100 and 150 (P<0.001), there was no significant difference between groups 200, 250, and 300 in the SOX9 protein. Meanwhile, group 250 exhibited the highest Col2a1 protein levels among the five different groups. Therefore, we believed that groups 200 or 250 might inhibit chondrocyte dedifferentiation better. Chondrocytes cultured in groups 100 and 150 could fill in the pores of the grids, rather than the cells in groups 200, 250, and 300. This phenomenon might weaken the effect of inhibiting chondrocyte dedifferentiation in 3D culture scaffolds with 100 and 150 μm spacing.

Discussion

OA is characterized by a progressive reduction in cartilage and lubricating synovia (38). Aging and trauma are risk factors for the development of OA (39,40). Due to the limited proliferative ability and avascularity, damaged cartilage cannot heal spontaneously (41). OA chondrocytes gradually lose their chondrogenic characteristics and display a fibroblast-like morphology during OA progression (42). The dedifferentiation and loss of chondrocyte phenotype occur during monolayer culturing (13). The maintenance of the chondrocyte phenotype has now emerged as the key to OA treatment. Therefore, chondrocytes in passage 2 were used in this study to mimic the progression of chondrocyte dedifferentiation in OA.

The expressions of *Col2a1* (43) and *SOX9* (44), which are markers of chondrocyte phenotype, are reduced after chondrocyte dedifferentiation. Meanwhile, the reduction of related components of ECM directly affects signalling and conduction of adhesion molecules (45-48). GAG, collagen type II, and AGG are the main components of ECM, the reduction of which affects the weight-loading ability of cartilage (49,50). Finally, dedifferentiated chondrocytes lose

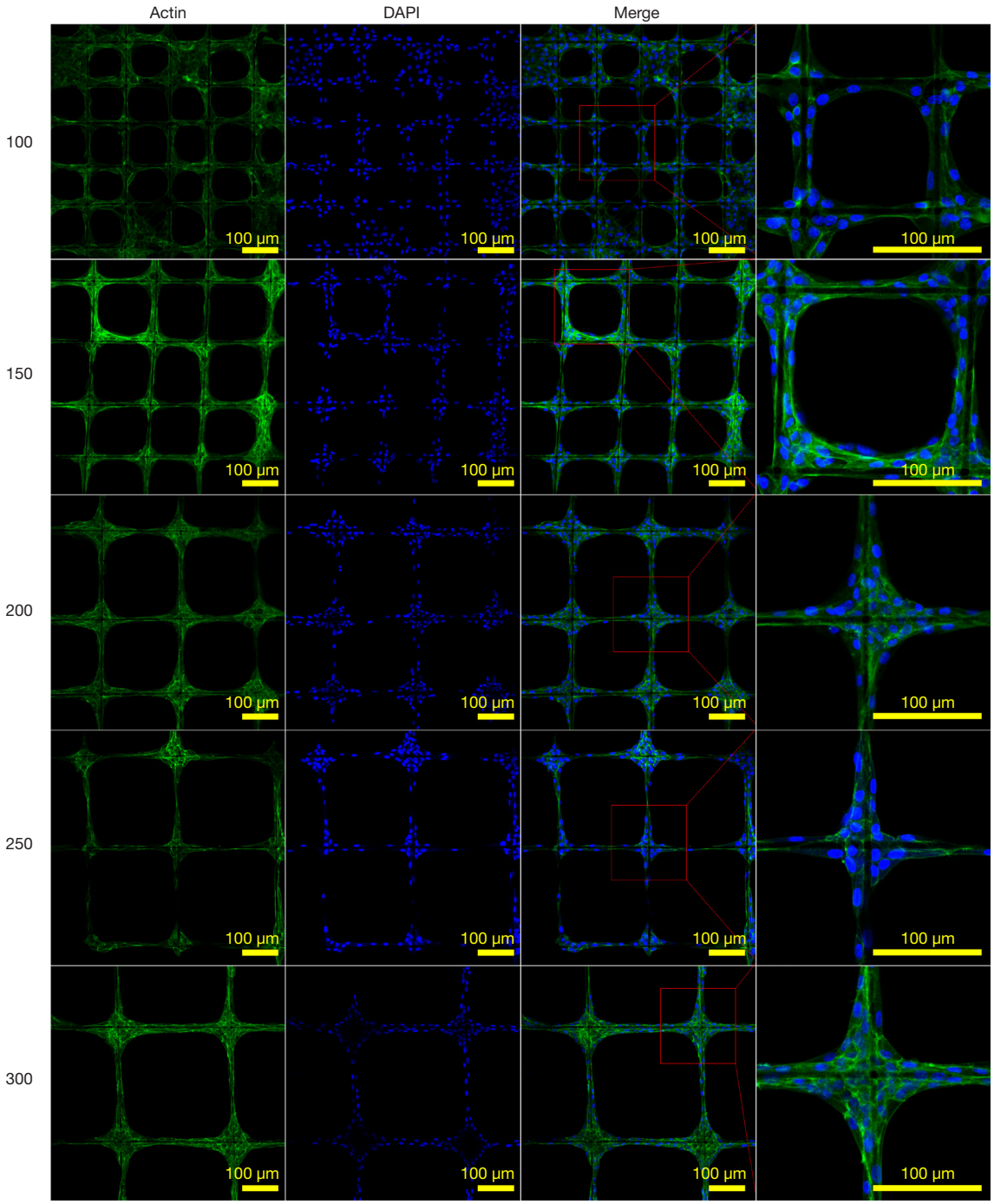

Figure 6 Fluorescent images of chondrocytes cultured on microfibrous structures with different spacing stained with iFluor™ 488 phalloidin and DAPI, with a scale bar of 100 μm. DAPI, 4',6-diamidino-2-phenylindole.

the ability to form normal cartilage (43,51,52).

Spacing is the main focus of our study. To determine whether larger or smaller spacing is better for maintaining the chondrocyte phenotype, groups with 100, 150, 200, 250, or 300 μm were established. In summary, chondrocytes were aggregated at the corner of the scaffolds and gradually extended on the microfibers. In groups 100 and 150, the cells could even fill in the square pores. This phenomenon is

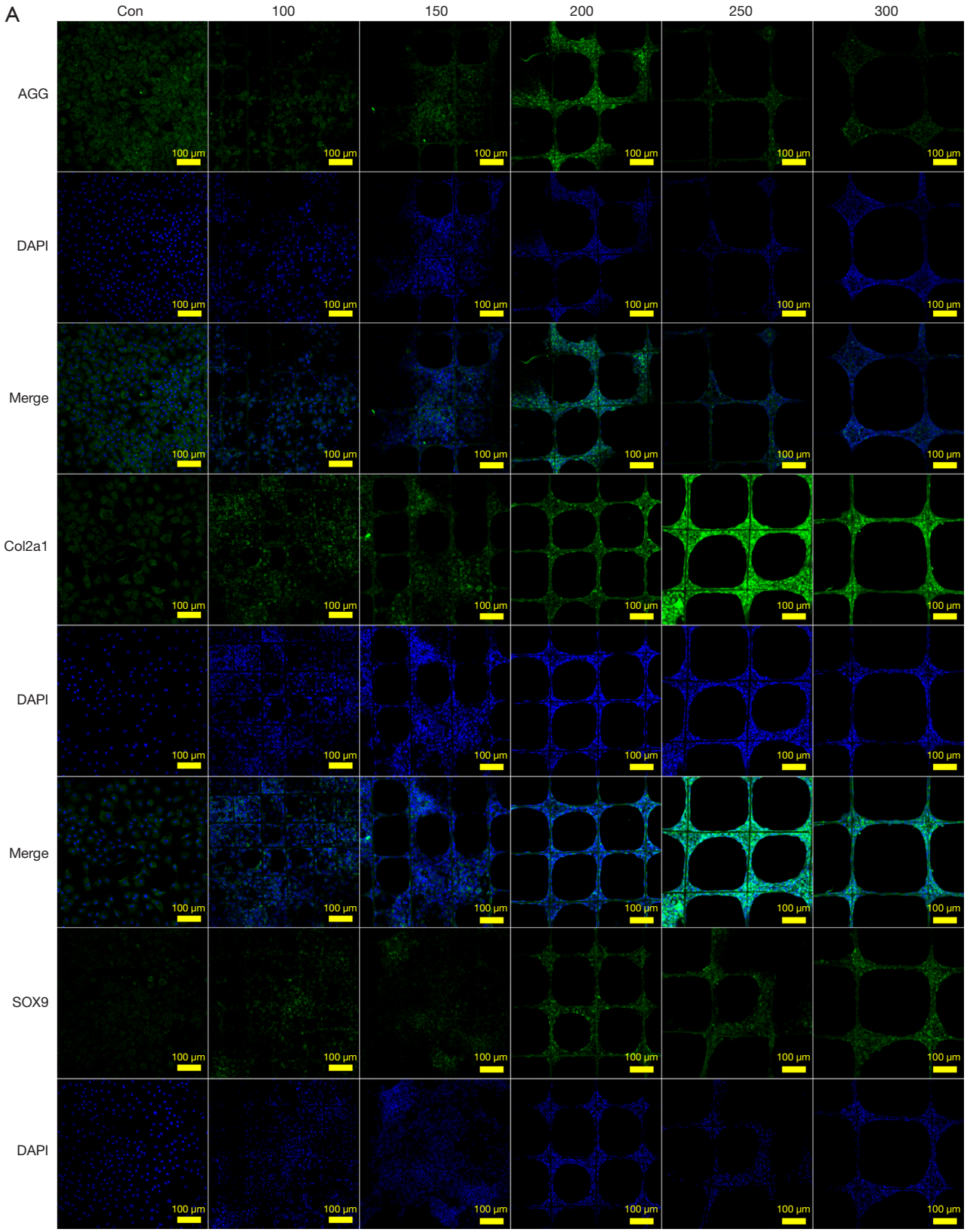

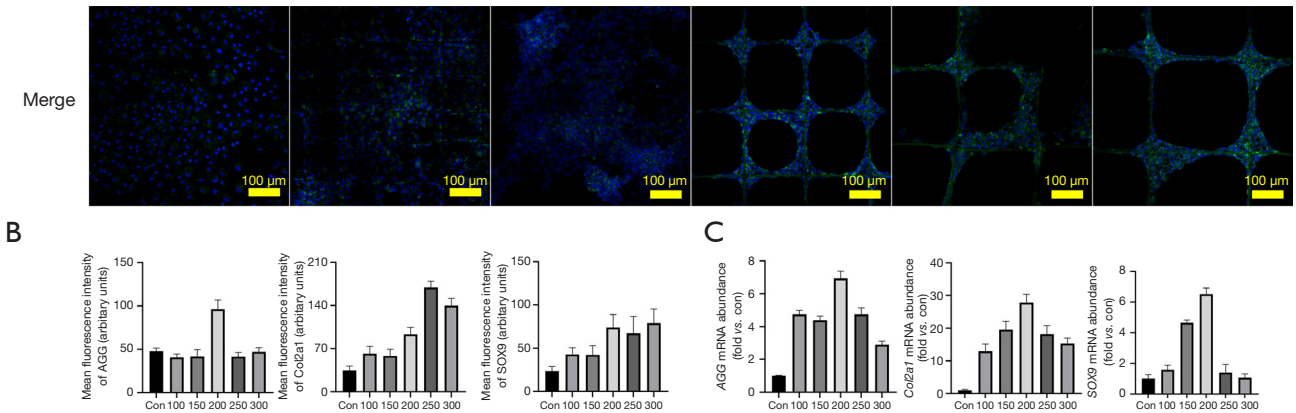

Figure 7 The expression levels of AGG, Col2a1, and SOX9 of chondrocytes in group Con, 100, 150, 200, 250 and 300 detected by immunofluorescence and qRT-PCR. Immunofluorescence images of chondrocytes cultured on microfibrous structures with different spacing, with a scale bar of 100 μm (A). Data are shown as mean ± SE, n=6–8 (B). The mRNA expression levels of *AGG*, *Col2a1*, and *SOX9* through qRT-PCR of chondrocytes cultured on microfibrous structures with different spacing. Data are shown as mean ± SE, n=3 (C). Con, control; AGG, aggrecan; DAPI, 4',6-diamidino-2-phenylindole; qRT-PCR, quantitative real-time polymerase chain reaction; SE, standard error; mRNA, messenger RNA.

similar to the findings of Lei *et al.* (53) in which cells showed a similar distribution tendency and general morphology to rice seedlings during growth. Due to the surface tension of liquid, seed cells are seeded at the corner of the grids and gradually migrate to the fibers, crossing vertical even parallel 2 fibers. Finally, proliferated cells filled in each pore of the grids. Moreover, groups 200, 250, and 300 were superior to groups 100 or 150 in terms of the GAG level, as well as the mRNA and protein levels of *AGG*, *Col2a1*, and *SOX9*. We speculated that small spacing (100 and 150 μm) might not be suitable for chondrocyte culturing. Chondrocytes in groups 100 and 150 could easily attach onto crossed vertical or parallel 2 fibers with an elongated cell shape, which was a different shape to chondrocytes in natural cartilage (*Figures 5*-7). Moreover, we found that chondrocytes were more susceptible to fill the pores completely, which demonstrated less of a difference with the monolayer culture. Meanwhile, the cells were gathered in the corner of pores with round or oval shapes in groups 200, 250, and 300, which is more likely with chondrocytes in natural cartilage. Thus, 200 μm is our recommended spacing, which was also verified in Prasopthum *et al.* (33) and Zhang *et al.* (34).

There are still multiple challenges for clinical application of 3D printed scaffolds. The method of printing, deposition of materials, determines low ability of stretchability for the scaffolds (54). Composite materials may be a good method dealing with this problem, but it is still a long way to go.

Conclusions

3D printed scaffolds with a spacing of 200 μm may serve as a potential candidate for chondrocyte expansion and the maintenance of chondrocyte phenotype, which would benefit CTE.

Acknowledgments

Funding: This work was supported by the National Natural Science Foundation of China (No. 31971272 and No. 31470936) and Sanming Project of Medicine in Shenzhen (No. SZSM201911011).

Footnote

Reporting Checklist: The authors have completed the MDAR reporting checklist. Available at https://atm.amegroups.com/article/view/10.21037/atm-22-2796/rc

Data Sharing Statement: Available at https://atm.amegroups.com/article/view/10.21037/atm-22-2796/dss

Conflicts of Interest: All authors have completed the ICMJE uniform disclosure form (available at https://atm.amegroups.com/article/view/10.21037/atm-22-2796/coif).

The authors have no conflicts of interest to declare.

Ethical Statement: The authors are accountable for all aspects of the work in ensuring that questions related to the accuracy or integrity of any part of the work are appropriately investigated and resolved. All animal experiments were approved by the Fourth Military Medical University Animal Ethics Committee (permission number: IACUC-20220701) and were implemented in accordance with the Guide for the Care and Use of Laboratory Animals (NIH, 8th edition).

References

1. Maihöfer J, Madry H, Rey-Rico A, et al. Hydrogel-Guided, rAAV-Mediated IGF-I Overexpression Enables Long-Term Cartilage Repair and Protection against Perifocal Osteoarthritis in a Large-Animal Full-Thickness Chondral Defect Model at One Year In Vivo. Adv Mater 2021;33:e2008451.
2. Kwon H, Brown WE, Lee CA, et al. Surgical and tissue engineering strategies for articular cartilage and meniscus repair. Nat Rev Rheumatol 2019;15:550-70.
3. da Costa BR, Pereira TV, Saadat P, et al. Effectiveness and safety of non-steroidal anti-inflammatory drugs and opioid treatment for knee and hip osteoarthritis: network meta-analysis. BMJ 2021;375:n2321.
4. Guermazi A, Hayashi D, Roemer FW, et al. Brief Report: Partial- and Full-Thickness Focal Cartilage Defects Contribute Equally to Development of New Cartilage Damage in Knee Osteoarthritis: The Multicenter Osteoarthritis Study. Arthritis Rheumatol 2017;69:560-4.
5. Cai G, Aitken D, Laslett LL, et al. Effect of Intravenous Zoledronic Acid on Tibiofemoral Cartilage Volume Among Patients With Knee Osteoarthritis With Bone Marrow Lesions: A Randomized Clinical Trial. JAMA 2020;323:1456-66.
6. Wang Z, Jones G, Winzenberg T, et al. Effectiveness of Curcuma longa Extract for the Treatment of Symptoms and Effusion-Synovitis of Knee Osteoarthritis : A Randomized Trial. Ann Intern Med 2020;173:861-9.
7. Roos EM, Arden NK. Strategies for the prevention of knee osteoarthritis. Nat Rev Rheumatol 2016;12:92-101.
8. Deyle GD, Allen CS, Allison SC, et al. Physical Therapy versus Glucocorticoid Injection for Osteoarthritis of the Knee. N Engl J Med 2020;382:1420-9.
9. Yeung P, Zhang W, Wang XN, et al. A human osteoarthritis osteochondral organ culture model for cartilage tissue engineering. Biomaterials 2018;162:1-21.
10. Brittberg M, Lindahl A, Nilsson A, et al. Treatment of deep cartilage defects in the knee with autologous chondrocyte transplantation. N Engl J Med 1994;331:889-95.
11. von der Mark K, Gauss V, von der Mark H, et al. Relationship between cell shape and type of collagen synthesised as chondrocytes lose their cartilage phenotype in culture. Nature 1977;267:531-2.
12. Yano F, Hojo H, Ohba S, et al. Cell-sheet technology combined with a thienoindazole derivative small compound TD-198946 for cartilage regeneration. Biomaterials 2013;34:5581-7.
13. Shao X, Lin S, Peng Q, et al. Tetrahedral DNA Nanostructure: A Potential Promoter for Cartilage Tissue Regeneration via Regulating Chondrocyte Phenotype and Proliferation. Small 2017. doi: 10.1002/smll.201602770.
14. Hubka KM, Dahlin RL, Meretoja VV, et al. Enhancing chondrogenic phenotype for cartilage tissue engineering: monoculture and coculture of articular chondrocytes and mesenchymal stem cells. Tissue Eng Part B Rev 2014;20:641-54.
15. Wuest SL, Caliò M, Wernas T, et al. Influence of Mechanical Unloading on Articular Chondrocyte Dedifferentiation. Int J Mol Sci 2018;19:1289.
16. Moroni L, Burdick JA, Highley C, et al. Biofabrication strategies for 3D in vitro models and regenerative medicine. Nat Rev Mater 2018;3:21-37.
17. Whitely M, Cereceres S, Dhavalikar P, et al. Improved in situ seeding of 3D printed scaffolds using cell-releasing hydrogels. Biomaterials 2018;185:194-204.
18. Lai Y, Cao H, Wang X, et al. Porous composite scaffold incorporating osteogenic phytomolecule icariin for promoting skeletal regeneration in challenging osteonecrotic bone in rabbits. Biomaterials 2018;153:1-13.
19. Cao H, Guan H, Lai Y, et al. Review of various treatment options and potential therapies for osteonecrosis of the femoral head. J Orthop Translat 2016;4:57-70.

20. He A, Ye A, Song N, et al. Phenotypic redifferentiation of dedifferentiated microtia chondrocytes through a three-dimensional chondrogenic culture system. Am J Transl Res 2020;12:2903-15.
21. Rakic R, Bourdon B, Hervieu M, et al. RNA Interference and BMP-2 Stimulation Allows Equine Chondrocytes Redifferentiation in 3D-Hypoxia Cell Culture Model: Application for Matrix-Induced Autologous Chondrocyte Implantation. Int J Mol Sci 2017;18:1842.
22. Park JU, Hardy M, Kang SJ, et al. High-resolution electrohydrodynamic jet printing. Nat Mater 2007;6:782-9.
23. Cho TH, Farjam N, Allemang CR, et al. Area-Selective Atomic Layer Deposition Patterned by Electrohydrodynamic Jet Printing for Additive Manufacturing of Functional Materials and Devices. ACS Nano 2020. [Epub ahead of print]. doi: 10.1021/acsnano.0c07297.
24. Shao F, Wan Q. Recent progress on jet printing of oxide-based thin film transistors. J Phys D Appl Phys 2019;52:143002.
25. Muldoon K, Song Y, Ahmad Z, et al. High Precision 3D Printing for Micro to Nano Scale Biomedical and Electronic Devices. Micromachines (Basel) 2022;13:642.
26. Rampichová M, Košt'áková Kuželová E, Filová E, et al. Composite 3D printed scaffold with structured electrospun nanofibers promotes chondrocyte adhesion and infiltration. Cell Adh Migr 2018;12:271-85.
27. Lee SJ, Heo DN, Park JS, et al. Characterization and preparation of bio-tubular scaffolds for fabricating artificial vascular grafts by combining electrospinning and a 3D printing system. Phys Chem Chem Phys 2015;17:2996-9.
28. Tam RY, Fuehrmann T, Mitrousis N, et al. Regenerative therapies for central nervous system diseases: a biomaterials approach. Neuropsychopharmacology 2014;39:169-88.
29. Rai V, Dilisio MF, Dietz NE, et al. Recent strategies in cartilage repair: A systemic review of the scaffold development and tissue engineering. J Biomed Mater Res A 2017;105:2343-54.
30. Muzzarelli RA, Greco F, Busilacchi A, et al. Chitosan, hyaluronan and chondroitin sulfate in tissue engineering for cartilage regeneration: a review. Carbohydr Polym 2012;89:723-39.
31. Sun Y, Wu Q, Zhang Y, et al. 3D-bioprinted gradient-structured scaffold generates anisotropic cartilage with vascularization by pore-size-dependent activation of HIF1α/FAK signaling axis. Nanomedicine 2021;37:102426.
32. Di Luca A, Szlazak K, Lorenzo-Moldero I, et al. Influencing chondrogenic differentiation of human mesenchymal stromal cells in scaffolds displaying a structural gradient in pore size. Acta Biomater 2016;36:210-9.
33. Prasopthum A, Cooper M, Shakesheff KM, et al. Three-Dimensional Printed Scaffolds with Controlled Micro-/Nanoporous Surface Topography Direct Chondrogenic and Osteogenic Differentiation of Mesenchymal Stem Cells. ACS Appl Mater Interfaces 2019;11:18896-906.
34. Zhang ZZ, Jiang D, Ding JX, et al. Role of scaffold mean pore size in meniscus regeneration. Acta Biomater 2016;43:314-26.
35. Lee CH, Cook JL, Mendelson A, et al. Regeneration of the articular surface of the rabbit synovial joint by cell homing: a proof of concept study. Lancet 2010;376:440-8.
36. Qu X, Xia P, He J, et al. Microscale electrohydrodynamic printing of biomimetic PCL/nHA composite scaffolds for bone tissue engineering. Mater Lett 2016;185:554-7.
37. Liu L, Liu C, Zhang H, et al. How to Identify the "LIVE/DEAD" States of Microbes Related to Biosensing. ACS Sens 2020;5:258-64.
38. Zhu J, Yang S, Qi Y, et al. Stem cell-homing hydrogel-based miR-29b-5p delivery promotes cartilage regeneration by suppressing senescence in an osteoarthritis rat model. Sci Adv 2022;8:eabk0011.
39. Wieland HA, Michaelis M, Kirschbaum BJ, et al. Osteoarthritis - an untreatable disease? Nat Rev Drug Discov 2005;4:331-44.
40. Jeon OH, Kim C, Laberge RM, et al. Local clearance of senescent cells attenuates the development of post-traumatic osteoarthritis and creates a pro-regenerative environment. Nat Med 2017;23:775-81.
41. Hong Y, Han Y, Wu J, et al. Chitosan modified Fe3O4/KGN self-assembled nanoprobes for osteochondral MR diagnose and regeneration. Theranostics 2020;10:5565-77.
42. Charlier E, Malaise O, Zeddou M, et al. Restriction of spontaneous and prednisolone-induced leptin production to dedifferentiated state in human hip OA chondrocytes: role of Smad1 and β-catenin activation. Osteoarthritis Cartilage 2016;24:315-24.
43. Cao B, Peng R, Li Z, et al. Effects of spreading areas and aspect ratios of single cells on dedifferentiation of chondrocytes. Biomaterials 2014;35:6871-81.
44. Haseeb A, Kc R, Angelozzi M, et al. SOX9 keeps growth plates and articular cartilage healthy by inhibiting chondrocyte dedifferentiation/osteoblastic redifferentiation. Proc Natl Acad Sci U S A

2021;118:e2019152118.
45. Miao Z, Lu Z, Wu H, et al. Collagen, agarose, alginate, and Matrigel hydrogels as cell substrates for culture of chondrocytes in vitro: A comparative study. J Cell Biochem 2018;119:7924-33.
46. Chen X, Gumbiner BM. Crosstalk between different adhesion molecules. Curr Opin Cell Biol 2006;18:572-8.
47. Knudson W, Loeser RF. CD44 and integrin matrix receptors participate in cartilage homeostasis. Cell Mol Life Sci 2002;59:36-44.
48. Weber GF, Bjerke MA, DeSimone DW. Integrins and cadherins join forces to form adhesive networks. J Cell Sci 2011;124:1183-93.
49. Sun M, Lu Z, Cai P, et al. Salidroside enhances proliferation and maintains phenotype of articular chondrocytes for autologous chondrocyte implantation (ACI) via TGF-β/Smad3 Signal. Biomed Pharmacother 2020;122:109388.
50. Robinson D, Ash H, Yayon A, et al. Characteristics of cartilage biopsies used for autologous chondrocytes transplantation. Cell Transplant 2001;10:203-8.
51. Dell'Accio F, De Bari C, Luyten FP. Molecular markers predictive of the capacity of expanded human articular chondrocytes to form stable cartilage in vivo. Arthritis Rheum 2001;44:1608-19.
52. Lin L, Zhou C, Wei X, et al. Articular cartilage repair using dedifferentiated articular chondrocytes and bone morphogenetic protein 4 in a rabbit model of articular cartilage defects. Arthritis Rheum 2008;58:1067-75.
53. Lei H, Yi T, Fan H, et al. Customized additive manufacturing of porous Ti6Al4V scaffold with micro-topological structures to regulate cell behavior in bone tissue engineering. Mater Sci Eng C Mater Biol Appl 2021;120:111789.
54. Duan Y, Ding Y, Bian J, et al. Ultra-Stretchable Piezoelectric Nanogenerators via Large-Scale Aligned Fractal Inspired Micro/Nanofibers. Polymers (Basel) 2017;9:714.

(English Language Editor: A. Kassem)

Cite this article as: Liu X, Zhang Z, Shi Y, Meng X, Qiu Z, Qu X, Dang J, Zhang Y, Sun L, Wang L, Zhu D, Mi Z, He J, Fan H. Effect of electrohydrodynamic printing scaffold with different spacing on chondrocyte dedifferentiation. Ann Transl Med 2022;10(13):743. doi: 10.21037/atm-22-2796

